Accepted Manuscript

Author: Hua-Jie Wang Ying Cao Le-Le Wu Sha-Sha Wu Ali Raza Nan Liu Jin-Ye Wang Teruo Miyazawa
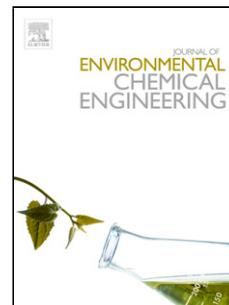
Please cite this article as: H.-J. Wang, Y. Cao, L.-L. Wu, S.-S. Wu, A. Raza, N. Liu, J.-Y. Wang, T. Miyazawa, ZnS-based dual nano-semiconductors (ZnS/PbS, ZnS/CdS or ZnS/Ag$_2$S,): a green synthesis route and photocatalytic comparison for removing organic dyes, *Journal of Environmental Chemical Engineering* (2018), https://doi.org/10.1016/j.jece.2018.10.034

This is a PDF file of an unedited manuscript that has been accepted for publication. As a service to our customers we are providing this early version of the manuscript. The manuscript will undergo copyediting, typesetting, and review of the resulting proof before it is published in its final form. Please note that during the production process errors may be discovered which could affect the content, and all legal disclaimers that apply to the journal pertain.

1 **Title Page**

2 **Title:**

3 ZnS-based dual nano-semiconductors (ZnS/PbS, ZnS/CdS or ZnS/Ag$_2$S,): a green

4 synthesis route and photocatalytic comparison for removing organic dyes

5 **Authors:**

6 Hua-Jie Wang [a, b], Ying Cao [c],Le-Le Wu [c], Sha-Sha Wu [c], Ali Raza[a], Nan Liu [c],

7 Jin-Ye Wang [a]*, Teruo Miyazawa [b]*

8 **Authors affiliations:**

9 [a] School of Biomedical Engineering, Shanghai Jiao Tong University, Dongchuan

10 Road, Shanghai 200240, P.R. China.

11 [b] New Industry Creation Hatchery Center (NICHe), Tohoku University, Sendai

12 980-0845, Japan.

13 [c] College of Chemistry and Chemical Engineering, Henan Normal University, 46

14 East of Construction Road, Xinxiang 453007, P.R. China.

15 *Corresponding author:

16 Name: Jin-Ye Wang

17 Address: School of Biomedical Engineering, Shanghai Jiao Tong University,

18 Dongchuan Road, Shanghai 200240, P.R. China.

19 Phone: +86-021-34205824

20 E-mail address: jinyewang@sjtu.edu.cn(J.Y. Wang)

21 Name: Teruo Miyazawa

22 Address: New Industry Creation Hatchery Center (NICHe), Tohoku University,

23 Sendai 980-0845, Japan.

24 E-mail address: miyazawa@m.tohoku.ac.jp(T. Miyazawa)

25 **Conflict of Interest**

1

1
2
3
4
5
6
7
8
9
10
11
12
13
14
15
16
17
18
19
20
21
22
23
24
25
26
27
28
29
30
31
32
33
34
35
36
37
38
39
40
41
42
43
44
45
46
47
48
49
50
51
52
53
54
55
56
57
58
59
60
61
62
63
64
65

26   The authors have no conflicts of interest.

27

2

Abstract

Organic dyes generating from many industries are considered as a potential source of water-pollution and have negative effects on human health. The present study was aimed to construct a green synthesis method for fabrication of ZnS-based dual nano-semiconductors and to compare the photocatalytic properties for removing cationic and anionic dyes. ZnS nanoparticles were synthesized using a template synthesis in Bovine Serum Albumin (BSA) solution and then ZnS/PbS, ZnS/CdS and ZnS/Ag$_2$S dual nano-semiconductors were prepared using ion-exchange method. Prepared nano-semiconductors were characterized by using HR-TEM, XRD, FTIR, TG/DTA and AAS. Moreover, photocatalytic activity of prepared nano-semiconductors was tested against Rhodamine B (cationic dye) and Methyl Orange (anionic dye). Results revealed that a controllable ZnS/PbS, ZnS/CdS and ZnS/Ag$_2$S ratio in nano-semiconductors can be achieved by adjusting the ion-exchange time. Prepared ZnS based composites exhibited higher photocatalytic efficiency than that of ZnS alone. In addition, photocatalytic activity of ZnS-based dual nano-semiconductors was found to be dependent upon composition and ratio of sulfides in nano-semiconductors with environmental pH. It was concluded that the combination of template synthesis and ion-exchange method is a feasible approach to fabricate new photocatalysts with higher photocatalytic activity.

3

1. Introduction

With every year passing, problem of water pollution is increasing because of industrialization. Industrial wastes contain different organic solvents, dyes, residues of products such as waste from pharmaceutical industry may contain drug or residues[1,2]. Out of them, dyes are rendering serious problems as they are not naturally degradable and difficult to degrade by using routine physical or chemical methods of water purification, however, these methods can reduce the concentration of these dyes[3]. Retention of these dyes in water can cause serious health problems such as methyl orange (MO), a widely used azo-dye, can induce DNA damage[4,5]. In addition to that, metabolite of methyl orange is more toxic and is one of the causes for intestinal tumor induction[6,7]. Therefore, it is necessary to remove such toxic organic dyes from water in order to reduce their health hazards. In this regard, photocatalysis process was emerged as a promising approach for degradation of such dyes[3]. In photocatalysis, free electron-hole pair generation due to light absorption lead to production of free radicals which have superior oxidizing property leading to decomposition of organic contaminants [8]. To achieve higher photocatalytic activity, photocatalysts are commonly employed during photocatalysis process, therefore; development of suitable photocatalysts is promising research area and different kinds of photocatalysts have been reported[9]. Metal sulfide nano-semiconductors have gathered a significant attention due to their exceptional chemical and physical characteristics[9].

Zinc sulfide (ZnS) is an II-VI compound semiconductor with a broader energy gap of 3.68 eV[10]. ZnS based semiconductors, being non-toxic, have been applied as photocatalyst for removal of organic contaminants through photodegradation process[9]. As a photocatalyst, it hasability to rapidly produce electron hole pair under

4

irradiation of light and also have been reported to have good photostability under UV light irradiation[9,11]. Nano-sized ZnS structures have shown enhanced photocatalytic activity due to enhanced surface area[12]. Doping technique to synthesize hybrid sulphides was reported to be one of feasible methods in order to enhance photocatalytic activity of ZnS. For instance, Wang et al. successfully synthesized ZnS/CdS core/shell nanotubes by combining hydrothermal treatment and ion exchange conversion. They found that the hybrid sulphide nanotubes exhibited about 11.02 and 5.56 times of photocatalytic rates than pure ZnS nanotubes and pure cadmium sulfide (CdS) nanotubles, respectively[13].In another report, C. Fenget al. synthesized ZnS/CuS nanowires with efficient photocatalytic activity against RhB and MO[14]. Different physicochemical process have been reported for production of ZnS based hybrid nanostructures such as co-precipitation, sol-gel process, thermal evaporation, solvothermal process, microemulsion etc[9,15]. Apart from ZnS and CdS, silver sulfide (Ag_2S) and lead sulfide (PbS) were also reported as photocatalyst in degradation of organic dyes[16]. In recent decade, green synthesis methods for synthesis of inorganic nanoparticles have gathered attention of many researchers in order to produce desired products using eco-friendly procedures[17].

In the present study, a green synthesis method was used to prepare ZnS based dual nano-semiconductors i.e. ZnS/Ag_2S, ZnS/PbS, ZnS/CdS. ZnS nanoparticles were synthesized by template synthesis using bovine serum albumin (BSA) followed by ion-exchange method to get different dual nano-semiconductors. Furthermore, their photocatalytic activity was compared against Rhodamine B (RhB) and methyl orange (MO). Photocatalytic activity was found to be dependent upon composition and ratio of hybrid sulfide nano-semiconductors which can be adjusted by varying ion-exchange time.

2. Experimental section

5

103 *2.1. Materials*

104   Zinc nitrate hexahydrate (>99%, MW=297.49, A.R.),silver nitrate ($\geqq$99.8%,

105 MW = 169.87 A.R.), cadmium chloride (>99.99%, MW=183.32, A.R.), lead nitrate

106 (>99.99%, MW=331.21, A.R.) and thioacetamide (TAA) ($\geqq$99.0%, Mw=75.13, A.R.)

107 were purchased from Tianjin Chemical Reagent Factory (Tianjin, China). BSA ($\geqq$

108 98%, Mw = 68,000) was purchased from sigma (St. Louis, MO, USA). All other

109 solvents and reagents used were of analytical grade.

110 *2.2. Green synthesis of ZnS-based nano-semiconductors*

111 *2.2.1. Template synthesis of ZnSnano-semiconductors*

112   ZnS nano-semiconductors were synthesized by a template method using BSA as

113 the structure-directing reagent. Briefly, 15 mL of 19.8 mg/mL zinc nitrate aqueous

114 solution was drop-wise added into 40 mL of 1.25 mg/mL BSA aqueous solution under

115 stirring. The mixture was kept static in dark for 12 h at 37 ℃. Following that, 15 mL

116 of 10 mg/mL TAA solution was drop-wise supplemented under stirring. The pH value

117 of the mixture was adjusted to 7.5 using NaOH (2 M) solution. After 3 days of

118 reaction at 37 ℃, the prepared sample was separated by centrifugation at 10,000 rpm

119 for 10 min. The collected product was washed with double distilled water and

120 lyophilized for 8 h.

121 *2.2.2. Ion exchange for controllable synthesis of dual nano-semiconductors*

122   ZnS-based dual nano-semiconductors were fabricated by the ion-exchange method.

123 Briefly, the prepared ZnS nano-semiconductors were dispersed into 25 mL of 40 mM

124 solutions of cadmium chloride, silver nitrate, lead nitrate solution, separately. The ion

125 exchange process was allowed to carry out at 37 ℃ for pre-determined time i.e.1, 3,

126 4 and 6 h. The final products were separated by centrifugation at 10,000 rpm for 10

127 min. The collected product was washed with double distilled water and lyophilized

6

128 for 8 h. These nano-semiconductors were named according to ion-exchange time.

129 *2.3. Characterization*

130 Content of nano-semiconductors was determined using atomic absorption

131 spectrometer. High-resolution transmission electron microscopy was used to observe

132 the size and crystal lattice structure (HR-TEM, JEM 2010, JEOL, Japan).

133 The presence and content of BSA in samples were measured using Fourier

134 transform infrared spectra (FTIR) and Thermo gravimetry-Differential Thermal

135 Analysis (TG/DTA). Potassium bromide pallets of samples were prepared with ratio

136 of 3:100 (sample:KBr) and FTIR spectra were recorded using Fourier transform

137 infra-red spectrophotometer (BIO-RAD, FTS-40, China) within wavenumber range of

138 4000-650 cm^{-1} at 2 cm^{-1} resolution with 128 scan. The TG/DTA thermograms were

139 recorded for each nanocomposite using TG/DTA analyzer(Seiko Instrument Inc.,

140 EXSTAR6300 TG/DTA, Japan) in presence of oxygen.

141 The XRD patterns were taken using Powder X-ray diffractometer (Bruker, D8

142 Advance, Germany) with graphite monochromatized graphite monochromatized

143 CuKα radiation (λ=0.15406 nm) between 2Θ angle range of 10-80° at 0.05^{o} s^{-1} scan

144 rate.

145 The ultraviolet-visible absorption and fluorescent spectra of different concentration

146 of prepared nano-semiconductors were measured at room temperature by UV-Vis

147 spectrophotometer (Beijing Purkinje General Instrument Co., Ltd., TU-11900, China)

148 and spectrofluorometer (JASCO , FP-6500, Japan).

149 *2.4. Photocatalytic activity of ZnS-based dual nano-semiconductors*

150 *2.4.1. Design of photocatalytic device*

151 The following photocatalytic experiments were carried out by using our in-house

152 made photo-catalysis device as shown in Fig. 1. This device contains four sections,

7

153 including light source, condensing system, 18 sample cells with magnetic stirrers. The

154 photocatalytic operation for different samples could be simultaneously performed,

155 which would avoid effect of any uncertain factor due to multiple experiments.

156 *2.4.2. Effect of environmental pH*

157 Both cationic (1.0×10^{-5} mol/L Rhodamine B, RhB) and anionic (1.0×10^{-5} mol/L

158 methyl orange, MO) dye solutions were prepared for the photo-degradation tests,

159 respectively (n=3). Briefly, the nano-semiconductors were dispersed into the organic

160 dye solution in a quartz glass tube, with a final concentration of 1 mg/mL. Here, the

161 pH values of the reactive system were maintained at 5.0, 6.0, 7.0, 8.0, and 9.0. After

162 illumination with 500 W of mercury lamp for the regular intervals, the kinetic

163 photo-decomposition process was described by measuring RhB concentration at 554

164 nm and MO concentrations at 464 nm, respectively, using UV-visible

165 spectrophotometer. As a control, dye solutions without any photo-catalyst were used

166 in order to evaluate the self-decomposition of dyes.

167 *2.4.3. Dye adsorption effect*

168 The dye adsorption on dual nano-semiconductors was evaluated in the dark

169 environment without illumination (n=3). The adsorption kinetic was quantified by

170 measuring RhB concentration at 554 nm and MO concentrations at 464 nm,

171 respectively, using UV visible spectrophotometer.

172 *2.4.4. Reycling of photocatalysts*

173 In order to study the recycling capability of ZnS-based dual nano-semiconductors,

174 photocatalytic activity of nano-semiconductors were evaluated for 5 cycles. The

175 initial concentration of dye was 1.0×10^{-5} mol/L and the pH value was set as 6.0.

176 Nano-semiconductors were obtained by centrifugation at 10,000 rpm for 10 min and

177 their photocatalytic ability against RhB and MO were determined.

8

3. Results and discussion

178

179   In this study, the combination of the template synthesis and ion exchange technique

180   was used to synthesize the ZnS-based dual nano-semiconductors. This study was

181   mainly based on the following advantages: (1) A synthetic route that allowed

182   fabrication of nano-composites under eco-friendly and gentle conditions, which will

183   reduce the dubious factors from organic system and investment cost from special

184   equipment. (2) The ion exchange technique which offered a facile method to

185   synthesize ZnS based nano-composite semiconductors in a controllable manner

186   without changing the initial morphology. (3) Comparison of photocatalytic activity of

187   different ZnS based nanocomposites against cationic and anionic dye.

188   *3.1. Green synthesis of ZnS-based dual nano-semiconductors*

189   From the typical HR-TEM and selected area electron diffraction (SAED) patterns of

190   ZnS/PbS$^{@1h}$, ZnS/CdS$^{@4h}$ and ZnS/Ag$_2$S$^{@2h}$ (Fig. 2), it can be seen that three kinds of

191   ZnS-based dual nano-semiconductors have well dispersity and less than 10 nm size in

192   diameter (Fig. 2A$_1$, Fig. 2B$_1$ and Fig. 2C$_1$). Both the clear lattice fringes in HR-TEM

193   and typical diffraction spots in the SAED images revealed that crystalline structure of

194   nano-semiconductors   (Fig.   2A$_1$-2C$_2$).   The   inorganic   components   in

195   nano-semiconductors were confirmed by XRD spectra. Before ion exchange, the

196   diffraction peaks for ZnS can be clearly distinguished and consistent with the values

197   of the standard (JCPDS 65-0309), with characteristic peaks at (2θ) 28.608°,

198   47.589°and 56.471°corresponding to (111), (220) and (311) crystal plane of

199   sphalerite, respectively (Fig. 2A$_3$). Because PbS (K_{sp}=8.0×10^{-28}), CdS (K_{sp}=8.0×10^{-27})

200   and Ag$_2$S (K_{sp}=6.3×10^{-50}) have the lower solubility product (K_{sp}) than ZnS

201   (2.93×10^{-25}), the ion-exchange method is feasible in theory to fabricate the hybrid

202   nano-semiconductors based on ZnS by ion-exchange method [18]With the increase in

9

203 ion exchange time, the diffraction peaks of PbS (standard JCPDS 05-0592), CdS

204 (standard JCPDS 41-1049) and Ag_2S (standard JCPDS 14-0072) were observed on

205 XRD patterns due to composite formation (PbS/ZnS, CdS/ZnS and Ag_2S/ZnS) as

206 shown in Fig. $2A_3$ to $2C_3$,. Moreover, diffraction peak intensities of PbS, CdS and

207 Ag_2S in corresponding nanocomposites were found to increase with further increase

208 in time of ion-exchange while intensities of ZnS related peaks was decreased due to

209 replacement of ions. The difference in solubility product (K_{sp}) of PbS, CdS and Ag_2S

210 results in the different ion-exchange rate, in order of $Ag_2S > PbS > CdS$.

211   The existence and content of BSA in ZnS-based dual nano-semiconductors was

212 measured by FTIR and TG/DTA. The FTIR results from Fig. 3A indicate that three

213 kinds of ZnS-based dual nano-semiconductors have the same FTIR spectra in the

214 range of 4000 cm^{-1}-600 cm^{-1}, characterizing with the stretching vibration of amide I

215 and amide II in the typical protein adsorption peaks at 1637 cm^{-1} and 1511 cm^{-1},

216 respectively. The TG measurement reveals the BSA content in ZnS/PbS$^{@1h}$,

217 ZnS/CdS$^{@4h}$ and ZnS/$Ag_2S^{@2h}$gets to 22.5%, 50.0% and 25.0%, respectively

218 corresponding to weight loss due to protein decomposition (Fig. $3B_1$-Fig. $3B_3$).

219   The UV-visible absorption spectra and fluorescent spectra of ZnS-based dual

220 nano-semiconductors were shown in Fig. 4A. It can be seen that ZnS/PbSand

221 ZnS/Ag_2S dual nano-semiconductors have a strong absorption in the UV-light region,

222 with an absorption peak at around 205nm. The UV absorption intensity increases with

223 the increase of sample contents. ZnS/CdS dual nano-semiconductors show two

224 absorption peaks at around 205 nm and 240 nm. The optical band gap of ZnS-based

225 dual nano-semiconductors was estimated from the Tauc plot and presented in the

226 insets of Fig.$4A_1$-Fig.$4A_3$[19]. From the absorption values, the calculated band gap is

227 5.68 eV for ZnS/PbS$^{@1h}$ and 5.59 eV for ZnS/$Ag_2S^{@2h}$ (the insets in Fig. $4A_1$ and A_3),

10

228 respectively. As for ZnS/CdS$^{@4h}$, there are two different band gaps, which are 4.41 eV

229 and 5.45 eV corresponding to CdS and ZnS, respectively. Figure 4B shows the

230 room-temperature PL spectral of ZnS/PbS$^{@1h}$ dual nano-semiconductors, ZnS/CdS$^{@4h}$

231 dual nano-semiconductors and ZnS/Ag$_2$S$^{@2h}$ dual nano-semiconductors. It is clear that

232 ZnS-based dual nano-semiconductors have the similar PL spectra of and exhibit

233 strong emission in the red region.

234 *3.2. Photocatalytic behaviors of dual nano-semiconductors*

235 Fig. 5 shows the heatmap of photocatalytic degradation of ZnS-based dual

236 nano-semiconductors againstRhodamine B and Methyl orange at different pH values.

237 pH is an important determining factor for dye degradation as it can increase/decrease

238 amount of reactive free radicals and also associated with dye-photocatalyst interaction

239 [20]. Overall, ZnS-based dual nano-semiconductors can effectively degrade both dyes

240 upon UV illumination. The photocatalytic efficiency of ZnS-based dual

241 nano-semiconductors was found in order of ZnS/CdS>ZnS/Ag$_2$S>ZnS/PbS>ZnS.

242 Moreover, the early ion-exchange products (e.g. ZnS/PbS$^{@1h}$, ZnS/CdS$^{@4h}$ and

243 ZnS/Ag$_2$S$^{@2h}$) have the highest photocatalytic efficiency than the later ion-exchange

244 products. The acid reactive system is more suitable for ZnS-based dual

245 nano-semiconductors to photo-degrade organic dyes.

246 It has been well documented that photocatalytic processes are based on the efficient

247 generation and separation process of carriers by means of band gap excitation[21].

248 Therefore, the generation and separation of the photo-induced electron-hole pairs are

249 the key factors to influence a photocatalytic reaction[22]. As for the pure ZnS, these

250 charge carriers might be rapidly recombined leading to a small fraction of the

251 available electrons and holes which can participate in the photocatalytic reaction

252 process [23]. Thus, pure ZnS samples have lower photocatalytic activity. However, in

11

253 case of dual nano-semiconductor photocatalysts, transfer of photo-generated charges

254 from one semiconductor into the lower lying energy bands of the second

255 semiconductor occurred by thermo-dynamical process [as shown in Scheme 1]. ZnS

256 has a wider band gap of ~3.7eV with about 2.5 eV of E_{vb} and -0.9 eVofE_{cb}. Both CdS

257 (E_g=~2.4 eV, E_{vb}=1.88 eV, E_{cb}=-0.52 eV) and Ag$_2$S (E_g=~1.0 eV, E_{vb}=1.0 eV, E_{cb}=0

258 eV) have narrow band gap [24,25].Their conduction and valence bands are located

259 within the energy gap of ZnS. Electron-hole pairs have tendency to localize within

260 CdS or Ag$_2$S, which provides the lowest energy states for both electrons and holes,

261 therefore, separation efficiency of photo-generated electrons and holes can be

262 improved. After that, ·OH radicals would be generated through the reaction between

263 valence band hole and water molecules (and hydroxyl) or by ·O$_2$, which is formed by

264 the combination of conduction band electron with adsorbed oxygen. Finally, ·O$_2$ and

265 ·OH radicals react with organic dyes to produce nontoxic products[26]. Therefore,

266 ZnS/CdS and ZnS/Ag$_2$S showed better catalytic activity than pure ZnS. As for

267 ZnS/PbS dual nano-semiconductor, it possibly performed the same photocatalytic

268 mechanism, and its photocatalytic activity was enhanced by comparison with that of

269 pure ZnS. However, the electrons of PbS could not transfer from conduction band of

270 ZnS to that of PbS due to the lower E_{cb} (-1.19 eV)[27]. Thus, ·O$_2$ couldn't be

271 generated and the degradation rate was decreased. Therefore, the photocatalytic

272 degradation rate on organic dyes of ZnS/PbS was lower than that of ZnS/CdS and

273 ZnS/Ag$_2$S.

274 In addition, ZnS-based dual nano-semiconductors exhibited higher photocatalytic

275 activity in acidic condition than in alkaline reactive system as represented by heat

276 map in Fig. 5. Furthermore, in order to compare different composites, kinetic analysis

277 of all composites was done at pH 6.0 against Rhodamine B and Methyl Orange which

12

278 showed that early ion-exchange products had better photocatalytic activity with order

279 of ZnS/CdS>ZnS/Ag$_2$S>ZnS/PbS>ZnS as shown in Fig. 6 and table 1 through

280 kinetic data analysis. Non-zero y-intercept as shown in Fig. 6 indicates involvement

281 of both dye adsorption and photocatalysis in remediation process. The photocatalytic

282 efficiency was found to be increased with decrease in pH within range of 5.0-9.0.

283 Variations in pH lead to changes in the ionization degree and surface properties of

284 ZnS-based nano-semiconductors [28]. Surfaces of photocatalysts exhibit positive

285 charge at low pH while negative charge at high pH [28,29]. In case of cationic dye

286 (Rhodamine B), protonation of ZnS based dual nano-semiconductors in the acid

287 reactive system caused the fewer dye adsorbed on its surface due to the electrostatic

288 repulsion, but there will form more hydroxyl on its surface. Therefore,

289 photo-generation of ·OH is considered as a key step for pH-dependent

290 photo-degradation of Rhodamine B by ZnS-based dual nano-semiconductors (Fig. 5).

291 In case of anionic dye (methyl orange), there are two possible reasonable explnations

292 for the pH-dependent photocatalytic behaviour of ZnS-based dual

293 nano-semiconductors (Fig. 5). On one hand, ZnS-based dual nano-semiconductors are

294 partially protonated due to the existence of BSA and thus able to electrostatically

295 interact with the anionic dye (Fig. 3) [30]. From Fig. 3 and Fig. 7, it can be seen that

296 ZnS/CdS dual nano-semiconductors had the most content of BSA, and thus the

297 highest methyl orange adsorption can be expected. In the dark, ZnS/CdS dual

298 nano-semiconductors showed the highest adsorption on methyl orange as depicted in

299 Fig.6. It means that ZnS/CdSdual nano-semiconductors can more effectively

300 photo-degrade methyl orange than ZnS/PbS and ZnS/Ag$_2$S dual nano-semiconductors.

301 Secondly, an increase in H$^+$ concentration always favours to promote methyl orange

302 forming a colourless hydrazine derivative in a dynamic sense [31]. Thus ZnS-based

13

303 dual nano-semiconductors have the higher photocatalytic activity in acid pH system

304 than in alkaline pH system.

305 $(CH_3)_2NC_6H_4N=NC_6H_4SO_3^- + 2H^+ + 2e^- \longrightarrow (CH_3)_2NC_6H_4NHNHC_6H_4SO_3^-$

306 Lastly, the effects of recycling on the photocatalytic activity were also investigated

307 while keeping the experimental conditions unchanged. Fig. 8 shows the repetitive

308 photo-degradation of RhB and MO during five consecutive cycles of reuse for

309 ZnS-based dual nano-semiconductors. The results showed that the photocatalytic

310 activity of all ZnS-based dual nano-semiconductors decreased significantly after five

311 cycles. The loss rate of photocatalytic activity on RhB is in order of

312 ZnS/CdS<ZnS/Ag$_2$S<ZnS/PbS<ZnS, which wereabout 28.7%, 35.4%, 51.1% and

313 63.0%, respectively. As for MO, the photocatalytic activity loss for ZnS/PbS,

314 ZnS/CdS and ZnS/Ag$_2$S dual nano-semiconductors are almost same i.e. 43.3%, 44.1%

315 and 42.2%, respectively. ZnS was found to loss more photdegadation activity (upto

316 61.2%) which is significantly higher than dual nano-semiconductors.

4. Conclusions

318 In summary, we successfully prepared ZnS-based dual nano-semiconductors by

319 combining the template synthesis technique and ion-exchange methods. The ratio of

320 dual sulphides in nano-semiconductors could be easily controlled by adjusting the

321 ion-exchange time. More importantly, the dual nano-semiconductors exhibited the

322 higher photocatalytic activity than pure ZnS. Moreover, the environmental pH and

323 adsorption activity of ZnS-based dual semiconductors are two key factors affecting

324 their photocatalytic activity. This data can serve as a guide for finding new

325 photocatalysts with higher photocatalytic activity on dye pollutants.

Acknowledgements

14

References

[1] P.D. Shivaramu, A. Patil, M. Murthy, S. Tubaki, M. Shastri, S. Manjunath, V. Gangaraju, D. Rangappa, Magnetic substrate supported ZnO-CuO nanocomposite as reusable photo catalyst for the degradation of organic dye, in: Mater. Today Proc., 2017: pp. 12314–12320. doi:10.1016/j.matpr.2017.09.165.

[2] K. He, G. Chen, G. Zeng, A. Chen, Z. Huang, J. Shi, T. Huang, M. Peng, L. Hu, Three-dimensional graphene supported catalysts for organic dyes degradation, Appl. Catal. B Environ. 228 (2018) 19–28. doi:10.1016/j.apcatb.2018.01.061.

[3] S. Natarajan, H.C. Bajaj, R.J. Tayade, Recent advances based on the synergetic effect of adsorption for removal of dyes from waste water using photocatalytic process, J. Environ. Sci. 65 (2018) 201–222. doi:10.1016/J.JES.2017.03.011.

[4] H. Ben Mansour, D. Barillier, D. Corroler, K. Ghedira, L. Chekir-Ghedira, R. Mosrati, In vitro study of DNA damage induced by acid orange 52 and its biodegradation derivatives., Environ. Toxicol. Chem. 28 (2009) 489–495. doi:10.1897/08-333.1.

[5] J. Feng, C.E. Cerniglia, H. Chen, Toxicological significance of azo dye metabolism by human intestinal microbiota., Front. Biosci. (Elite Ed). 4 (2012) 568–586. http://www.ncbi.nlm.nih.gov/pubmed/22201895.

[6] K.T. Chung, The significance of azo-reduction in the mutagenesis and carcinogenesis of azo dyes, Mutat. Res. Genet. Toxicol. 114 (1983) 269–281. doi:10.1016/0165-1110(83)90035-0.

[7] K.T. Chung, S.E. Stevens, C.E. Cerniglia, The reduction of azo dyes by the intestinal microflora, Crit. Rev. Microbiol. 18 (1992) 175–190. doi:10.3109/10408419209114557.

[8] H. You, Z. Wu, Y. Jia, X. Xu, Y. Xia, Z. Han, Y. Wang, High-efficiency and mechano-/photo- bi-catalysis of piezoelectric-ZnO@ photoelectric-TiO2core-shell nanofibers for dye decomposition, Chemosphere. 183 (2017) 528–535. doi:10.1016/j.chemosphere.2017.05.130.

[9] D. Ayodhya, G. Veerabhadram, A review on recent advances in photodegradation of dyes using doped and heterojunction based semiconductor metal sulfide nanostructures for environmental protection, Mater. Today Energy. 9 (2018) 83–113. doi:10.1016/j.mtener.2018.05.007.

15

365   [10]   R. Chauhan, A. Kumar, R. Pal Chaudhary, Photocatalytic degradation of
366   methylene blue with Cu doped ZnS nanoparticles, J. Lumin. 145 (2014) 6–12.
367   doi:10.1016/j.jlumin.2013.07.005.

368   [11]   J. Zhang, Y. Wang, J. Zhang, Z. Lin, F. Huang, J. Yu, Enhanced photocatalytic
369   hydrogen production activities of Au-loaded ZnS flowers, ACS Appl. Mater.
370   Interfaces. 5 (2013) 1031–1037. doi:10.1021/am302726y.

371   [12]   S. Talebi, N. Chaibakhsh, Z. Moradi-Shoeili, Application of nanoscale
372   ZnS/TiO2 composite for optimized photocatalytic decolorization of a textile
373   dye, J. Appl. Res. Technol. 15 (2017) 378–385. doi:10.1016/j.jart.2017.03.007.

374   [13]   Z. Wang, H. Zhang, H. Cao, L. Wang, Z. Wan, Y. Hao, X. Wang, Facile
375   preparation of ZnS/CdS core/shell nanotubes and their enhanced photocatalytic
376   performance, Int. J. Hydrogen Energy. 42 (2017) 17394–17402.
377   doi:10.1016/j.ijhydene.2017.04.091.

378   [14]   C. Feng, X. Meng, X. Song, X. Feng, Y. Zhao, G. Liu, Controllable synthesis
379   of hierarchical CuS/ZnS hetero-nanowires as high-performance visible-light
380   photocatalysts, RSC Adv. 6 (2016) 110266–110273. doi:10.1039/c6ra20306j.

381   [15]   W.Q. Peng, G.W. Cong, S.C. Qu, Z.G. Wang, Synthesis and photoluminescence
382   of ZnS:Cu nanoparticles, Opt. Mater. (Amst). 29 (2006) 313–317.
383   doi:10.1016/j.optmat.2005.10.003.

384   [16]   A. Dasari, V. Guttena, Green synthesis, characterization, photocatalytic,
385   fluorescence and antimicrobial activities of Cochlospermum gossypium capped
386   Ag<inf>2</inf>S nanoparticles, J. Photochem. Photobiol. B Biol. 157 (2016).
387   doi:10.1016/j.jphotobiol.2016.02.002.

388   [17]   K. Parveen, V. Banse, L. Ledwani, Green synthesis of nanoparticles: Their
389   advantages and disadvantages, in: AIP Conf. Proc., 2016.
390   doi:10.1063/1.4945168.

391   [18]   X. Yang, H. Xue, J. Xu, X. Huang, J. Zhang, Y.B. Tang, T.W. Ng, H.L. Kwong,
392   X.M. Meng, C.S. Lee, Synthesis of porous ZnS:Ag2S nanosheets by ion
393   exchange for photocatalytic H2generation, ACS Appl. Mater. Interfaces. (2014).
394   doi:10.1021/am5020953.

395   [19]   J. Tauc, A. Menth, States in the gap, J. Non. Cryst. Solids. 8–10 (1972)
396   569–585. doi:https://doi.org/10.1016/0022-3093(72)90194-9.

397   [20]   T.S. Natarajan, M. Thomas, K. Natarajan, H.C. Bajaj, R.J. Tayade, Study on
398   UV-LED/TiO2 process for degradation of Rhodamine B dye, Chem. Eng. J.
399   169 (2011) 126–134. doi:10.1016/j.cej.2011.02.066.

400   [21]   C.D. Pomar, A.T. Souza, G. Sombrio, F.L. Souza, J.J. Bonvent, J.A. Souza,
401   Synthesis of SnS and ZnS Hollow Microarchitectures Decorated with
402   Nanostructures and Their Photocatalytic Behavior for Dye Degradation,
403   ChemistrySelect. 3 (2018) 3774–3780. doi:10.1002/slct.201800383.

404   [22]   Z. Wu, L. Chen, C. Xing, D. Jiang, J. Xie, M. Chen, Controlled synthesis of
405   Bi2S3/ZnS microspheres by an in situ ion-exchange process with enhanced
406   visible light photocatalytic activity, Dalt. Trans. 42 (2013) 12980.
407   doi:10.1039/c3dt50984b.

408   [23]   H. Li, F. Xie, W. Li, H. Yang, R. Snyders, M. Chen, W. Li, Preparation and

16

409   Photocatalytic Activity of Ag2S/ZnS Core–Shell Composites, Catal. Surv. from
410   Asia. 22 (2018) 156–165. doi:10.1007/s10563-018-9249-2.

411 [24] G. Murugadoss, R. Jayavel, M. Rajesh Kumar, R. Thangamuthu, Synthesis,
412   optical, photocatalytic, and electrochemical studies on Ag2S/ZnS and
413   ZnS/Ag2S nanocomposites, Appl. Nanosci. 6 (2016) 503–510.
414   doi:10.1007/s13204-015-0448-0.

415 [25] C. Yang, Z.F. Zhou, J.W. Li, X.X. Yang, W. Qin, R. Jiang, N.G. Guo, Y. Wang,
416   C.Q. Sun, Correlation between the band gap, elastic modulus, Raman shift and
417   melting point of CdS, ZnS, and CdSe semiconductors and their size
418   dependency, Nanoscale. 4 (2012) 1304–1307. doi:10.1039/c2nr11605g.

419 [26] Z. Xin, L. Li, W. Zhang, T. Sui, Y. Li, X. Zhang, Synthesis of ZnS@CdS–Te
420   composites with p–n heterostructures for enhanced photocatalytic hydrogen
421   production by microwave-assisted hydrothermal method, Mol. Catal. 447
422   (2018) 1–12. doi:10.1016/j.mcat.2018.01.001.

423 [27] W. Cui, S. Ma, L. Liu, Y. Liang, PbS-sensitized K2Ti4O9composite:
424   Preparation and photocatalytic properties for hydrogen evolution under visible
425   light irradiation, Chem. Eng. J. 204–205 (2012) 1–7.
426   doi:10.1016/j.cej.2012.07.075.

427 [28] M. Ghaedi, H.A. Larki, S.N. Kokhdan, F. Marahel, R. Sahraei, A. Daneshfar,
428   M.K. Purkait, Synthesis and characterization of zinc sulfide nanoparticles
429   loaded on activated carbon for the removal of methylene blue, Environ. Prog.
430   Sustain. Energy. (2013). doi:10.1002/ep.11654.

431 [29] N. Soltani, E. Saion, M.Z. Hussein, M. Erfani, A. Abedini, G. Bahmanrokh, M.
432   Navasery, P. Vaziri, Visible light-induced degradation of methylene blue in the
433   presence of photocatalytic ZnS and CdS nanoparticles, Int. J. Mol. Sci. (2012).
434   doi:10.3390/ijms131012242.

435 [30] Q. Yang, R. Lu, S.S. Ren, C. Chen, Z. Chen, X. Yang, Three dimensional
436   reduced graphene oxide/ZIF-67 aerogel: Effective removal cationic and anionic
437   dyes from water, Chem. Eng. J. 348 (2018) 202–211.
438   doi:10.1016/j.cej.2018.04.176.

439 [31] L. Zang, C.Y. Liu, X.M. Ren, Photochemistry of semiconductor particles 3.
440   Effects of surface charge on reduction rate of methyl orange photosensitized by
441   ZnS sols, J. Photochem. Photobiol. A Chem. 85 (1995) 239–245.
442   doi:10.1016/1010-6030(94)03918-K.

443
444

17

445 Table 1. The kinetic rate constants of rhodamine B and methyl orange degradation

446 over the samples under UV irradiation.

Sample	Rhodamine B rate constants	Methyl orange rate constants
ZnS	0.0008	0.0008
ZnS/PbS$^{@1h}$	0.0035	0.0025
ZnS/PbS$^{@3h}$	0.0036	0.0023
ZnS/PbS$^{@4h}$	0.0037	0.0020
ZnS/PbS$^{@6h}$	0.0048	0.0018
ZnS/CdS$^{@4h}$	0.011	0.0062
ZnS/CdS$^{@12h}$	0.0094	0.0066
ZnS/CdS$^{@24h}$	0.0093	0.0053
ZnS/CdS$^{@48h}$	0.0083	0.0064
ZnS/Ag$_2$S$^{@2h}$	0.0057	0.0014
ZnS/Ag$_2$S$^{@4h}$	0.0052	0.0017
ZnS/Ag$_2$S$^{@8h}$	0.0047	0.0013
ZnS/Ag$_2$S$^{@24h}$	0.0044	0.0008

447

448
449

450

18

Figure legends

451

452 Figure 1. In-house made photo-catalysis device equipped with 18 sample cells.

453 Figure 2. HRTEM (1) and SAED images (2), and XRD patterns (3) of ZnS-based dual

454 nano-semiconductors. (A) ZnS/PbS$^{@1h}$, (B) ZnS/CdS$^{@4h}$ and (C) ZnS/Ag$_2$S$^{@2h}$.

455 Figure 3. FTIR (A) and TG/DTA (B) analysis of ZnS-based dual semiconductors (1)

456 ZnS/PbS$^{@1h}$, (2) ZnS/CdS$^{@4h}$ and (3) ZnS/Ag$_2$S$^{@2h}$.

457 Figure 4. UV-vis absorption spectra (A) and PL spectra (B) of ZnS-based dual

458 nano-semiconductors with different concentrations in aqueous solution. (1)

459 ZnS/PbS$^{@1h}$, (2) ZnS/CdS$^{@4h}$ and (3) ZnS/Ag$_2$S$^{@2h}$. The insets show the Tauc

460 plots of $(\alpha h v)^2$ *vs.* photon energy (hv) for ZnS-based dual

461 nano-semiconductors.

462 Figure 5. Heatmap of photocatalytic degradation rates of ZnS-based dual

463 nano-semiconductors on Rhodamine B and Methyl orange at different pH

464 values.

465 Figure 6. Degradation kinetics profiles of ZnS-based dual nano-semiconductors on

466 Rhodamine B (1) and Methyl orange (2). (A) ZnS/PbS, (B) ZnS/CdSand (C)

467 ZnS/Ag$_2$S.

468 Figure 7. Dark adsorption of ZnS and ZnS-based dual nano-semiconductors (all

469 ion-exchange products) on Rhodamine B (1) and Methyl orange (2) after 2 h.

470 Figure 8. Cycling degradation efficiency of ZnS-based dual nano-semiconductors on

471 Rhodamine B (1) and Methyl orange (2). (A) ZnS/PbS, (B) ZnS/CdSand (C)

472 ZnS/Ag$_2$S.

19

473   Scheme 1

474
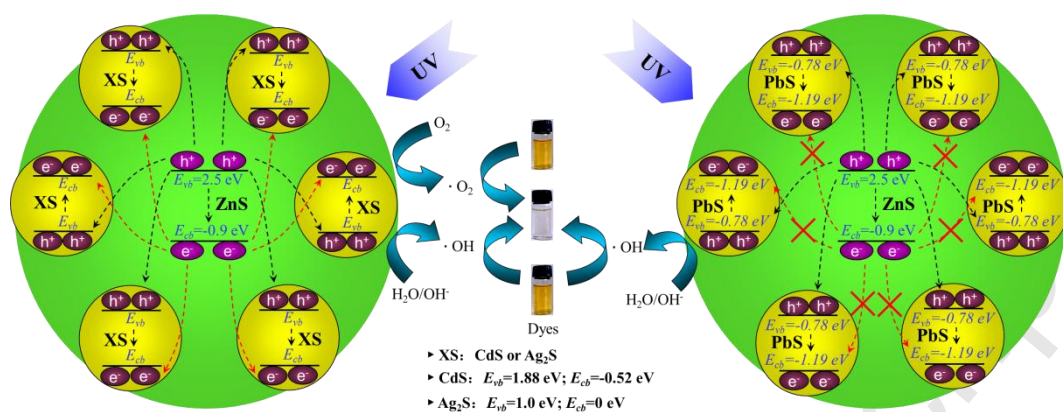
Scheme 1. A proposed photo-catalytic mechanism of ZnS-based dual

nano-semiconductors for degradation of organic dyes.

478

479

480 **Figure 1**

Condensate water

Mercury lamp

Magnetic stirrer

481

482

21

483 **Figure 2**

488   **Figure 3**

A

B$_1$

B$_2$
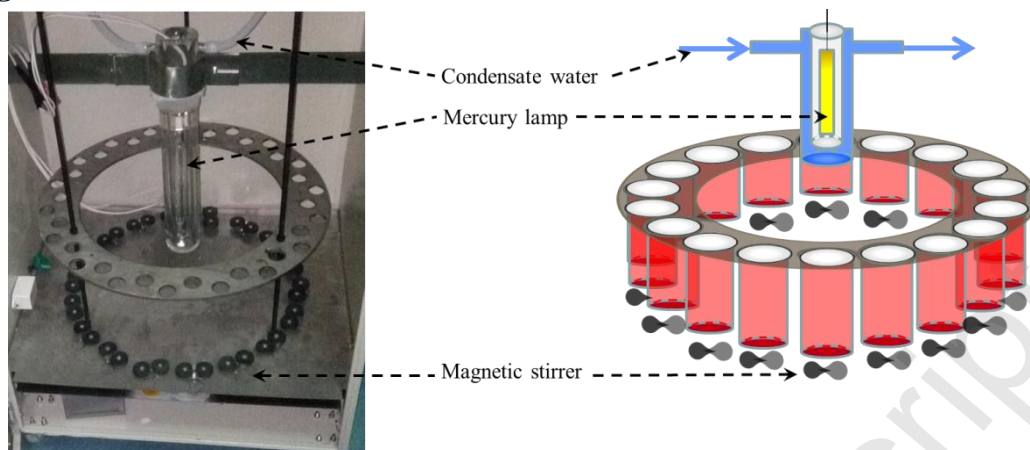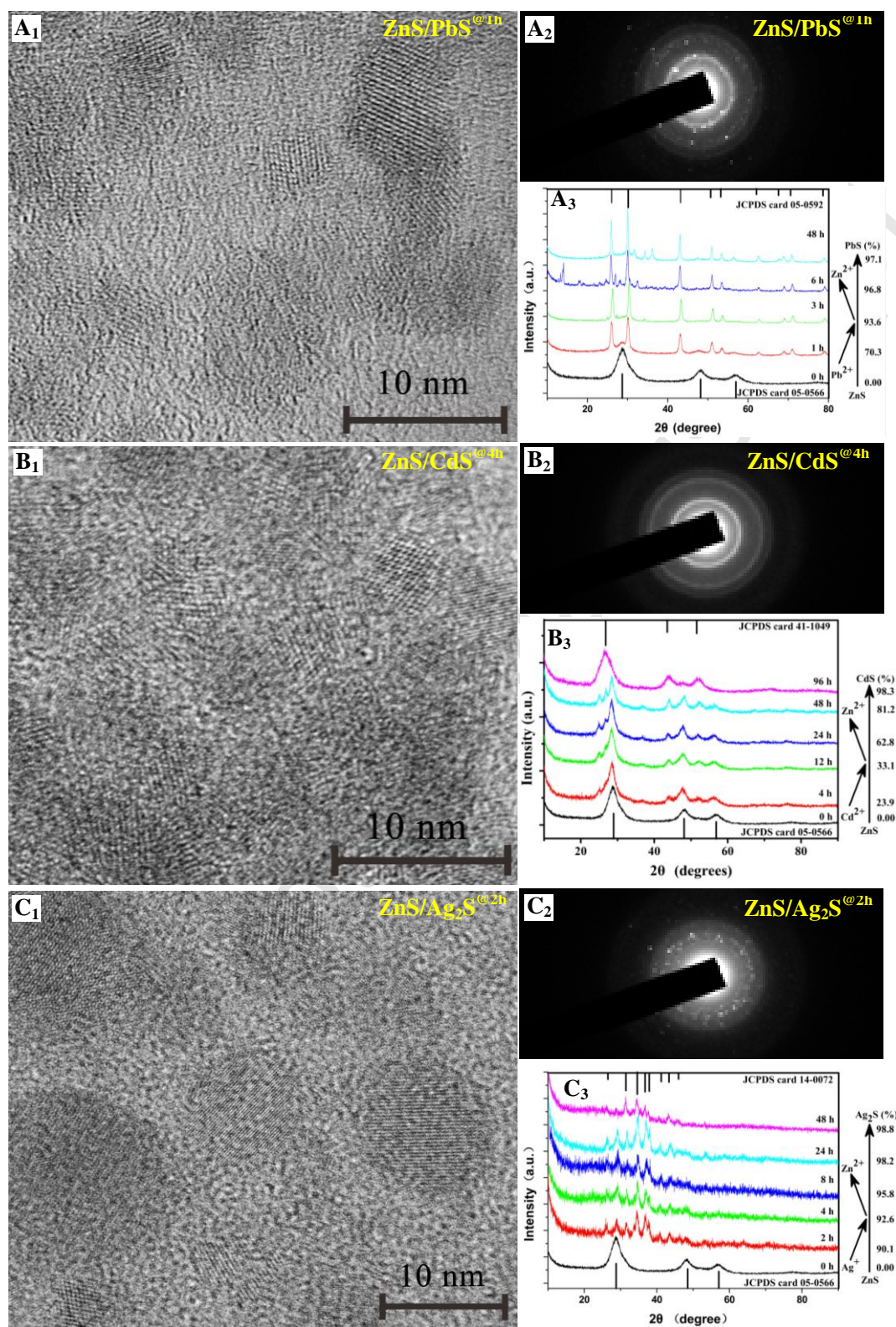
B$_3$
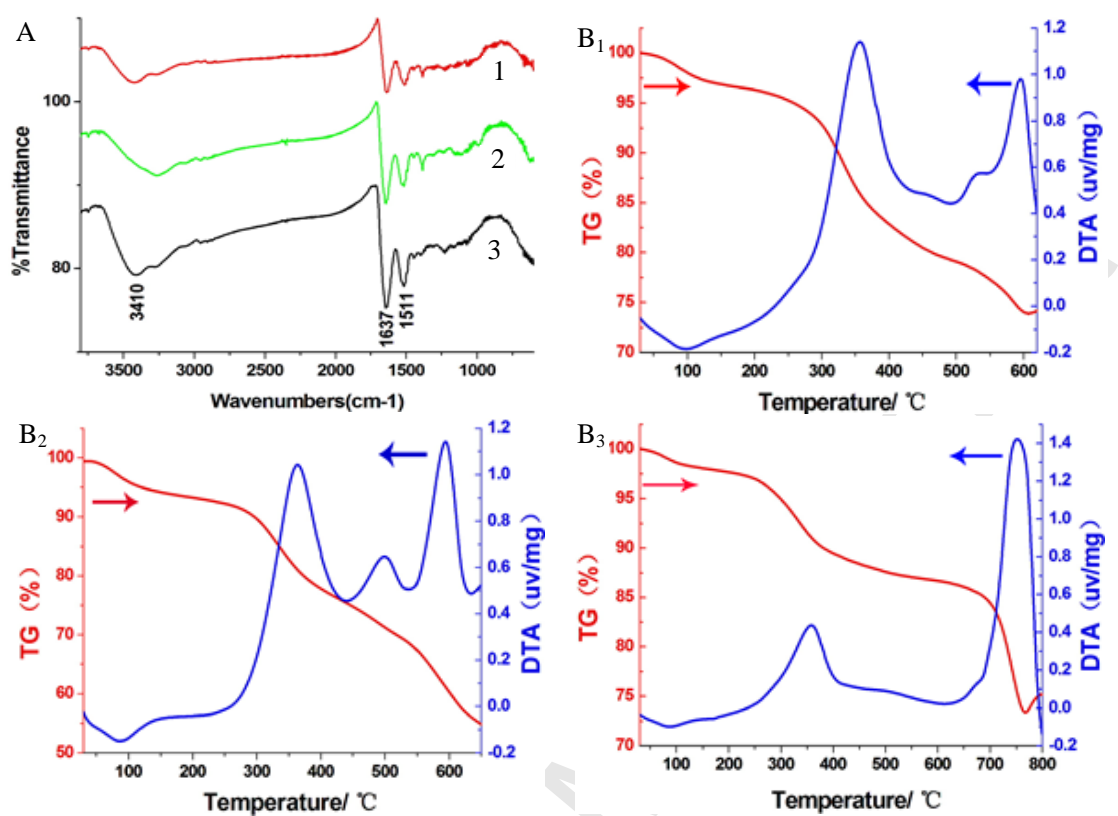
489

490

491 **Figure 4**

492

493

Figure 5

Rhodamine B   Methyl orange
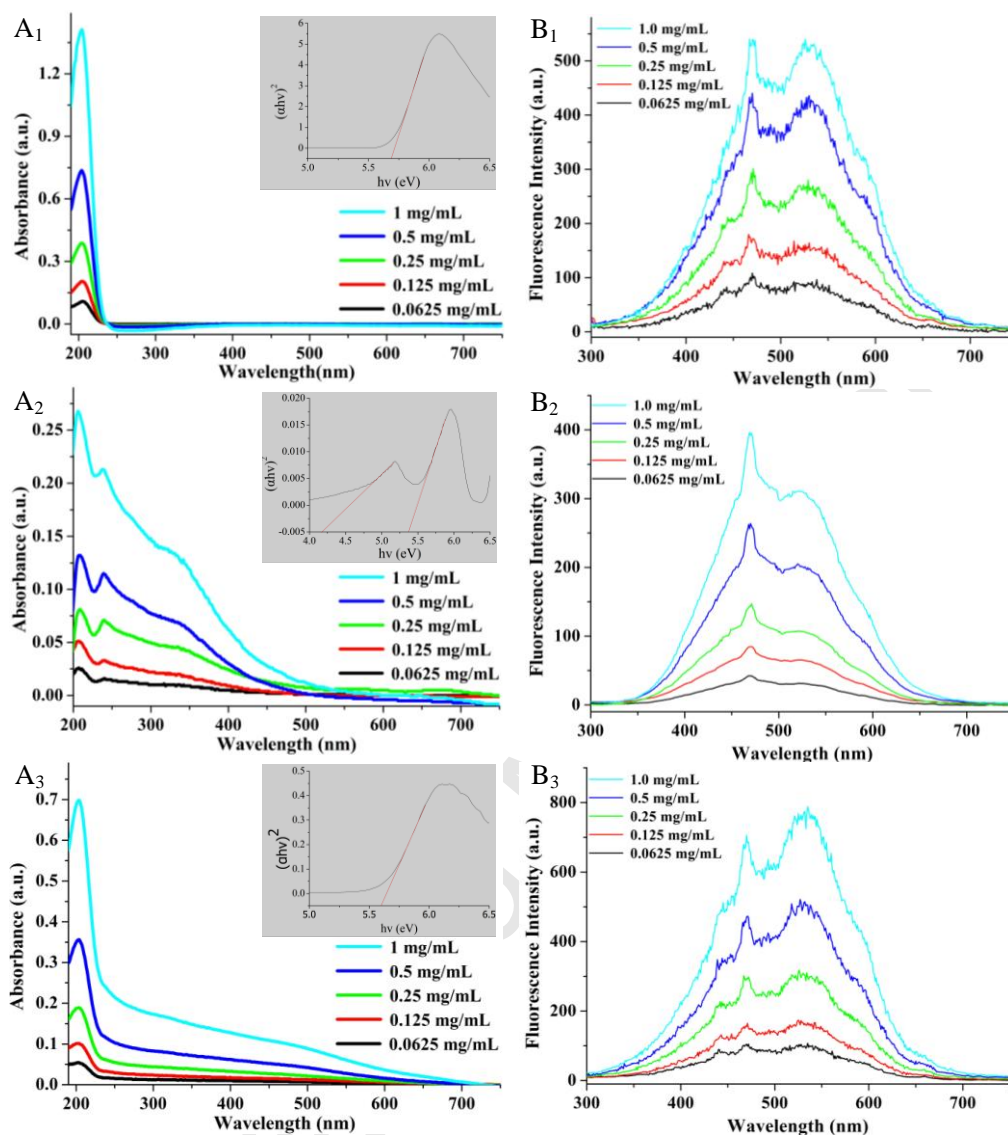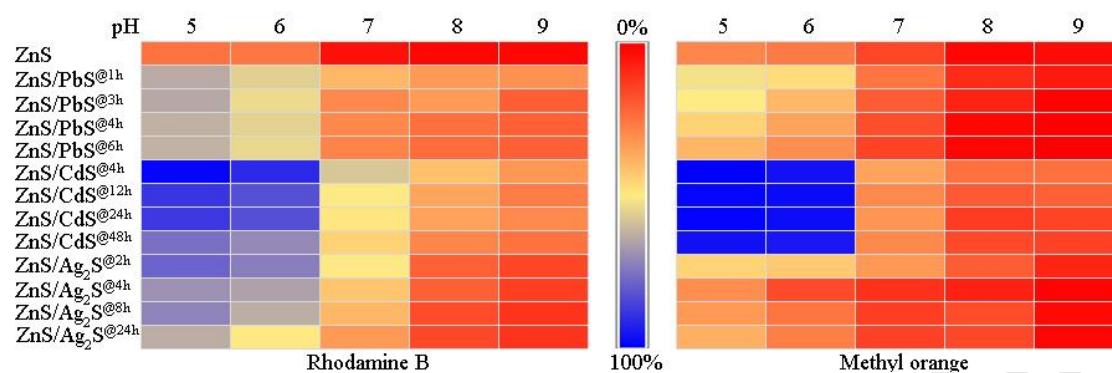
500 **Figure 6**
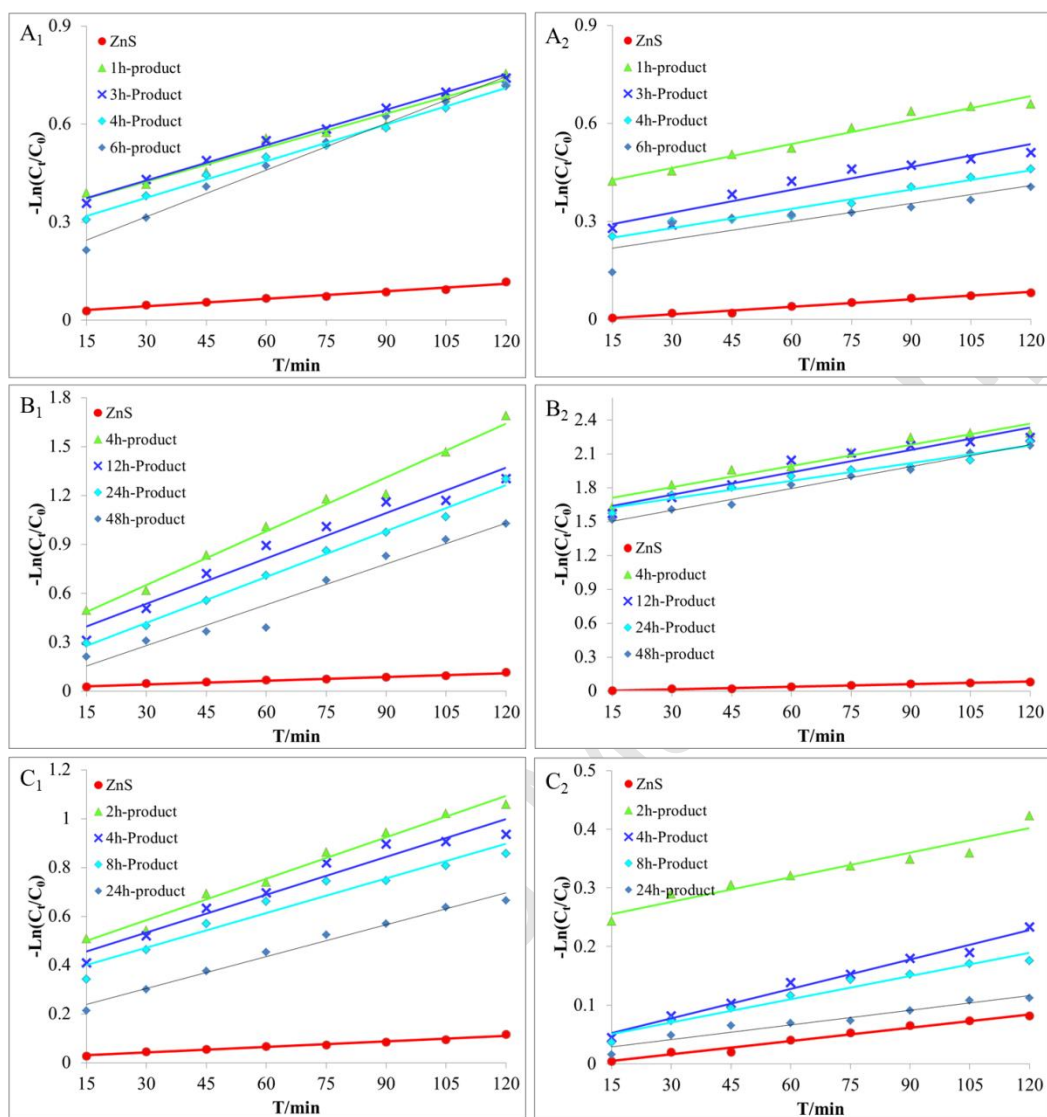
501

502

503

504

505 **Figure 7**
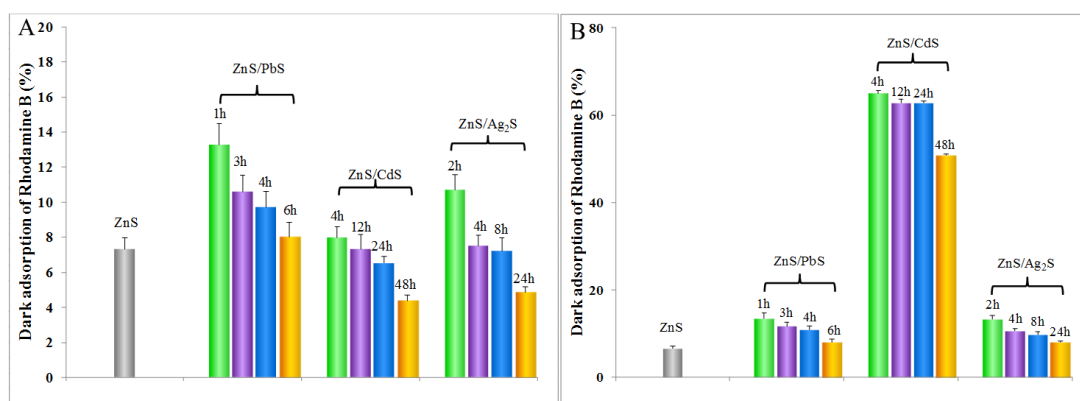
506

507

508

509 **Figure 8**

510

511

512

- XS: CdS or Ag₂S
- CdS: E_{vb}≈1.88 eV; E_{cb}≈-0.52 eV
- Ag₂S: E_{vb}=1.0 eV; E_{cb}=0 eV
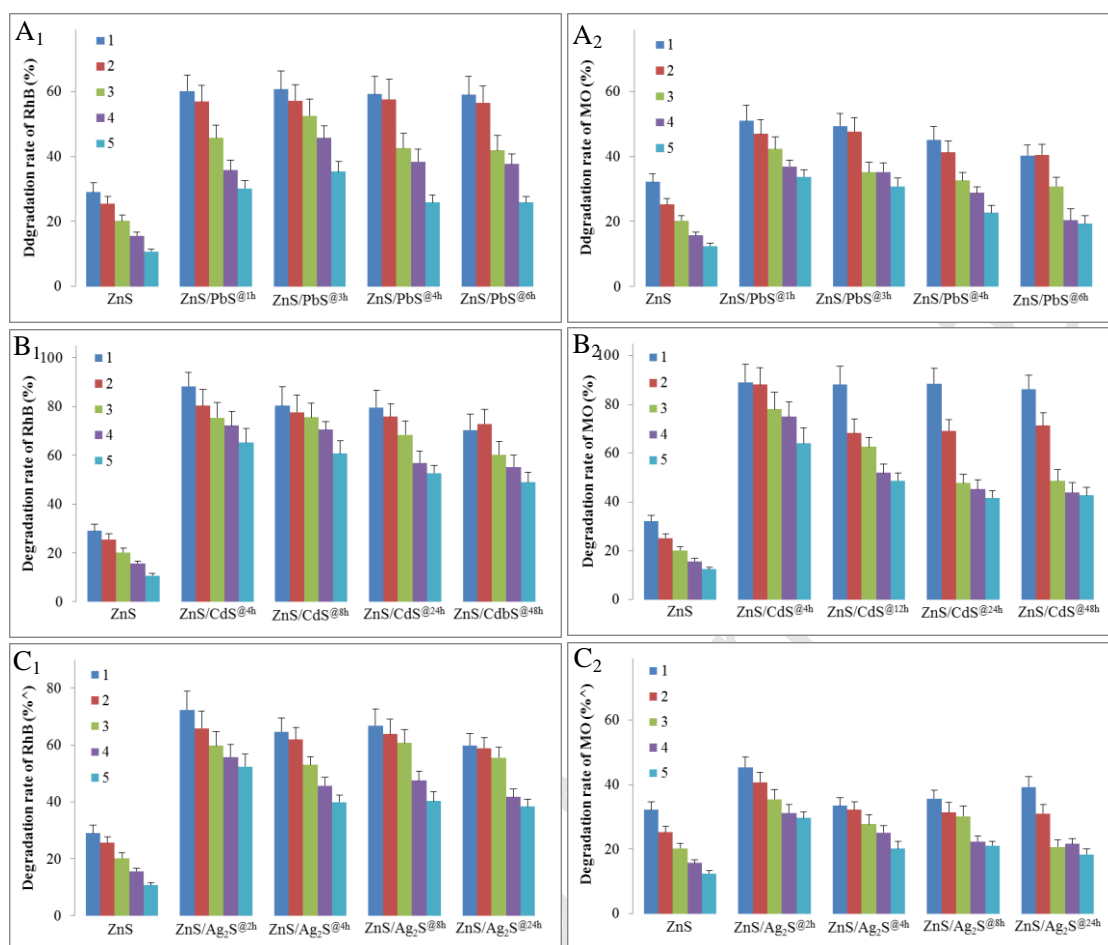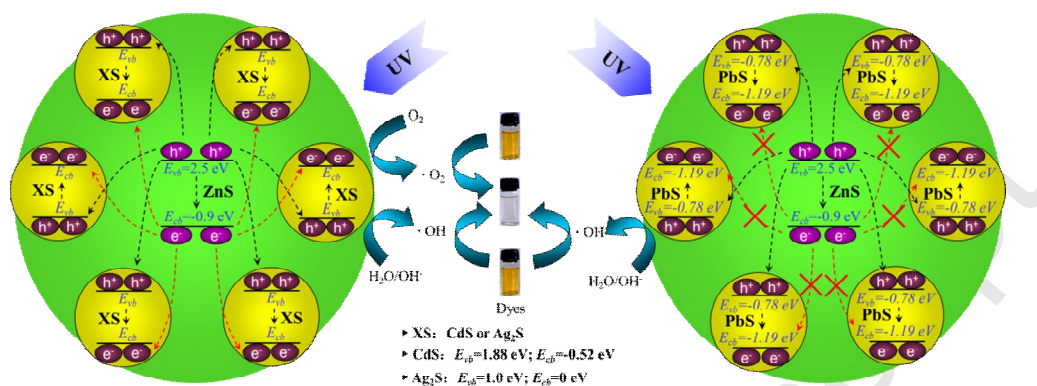
ZnS-based dual nano-semiconductors were successfully synthesized by combining the biomimetic technique and ion-exchange methods. The ratio of dual sulphides in nano-semiconductors was controllable and key factors improving the photocatalytic activity of ZnS photocatalyst.

1

- ➢ The green route was developed to prepare ZnS-based dual nano-semiconductors.

- ➢ The catalytic activity of dual nano-semiconductors was higher than pure ZnS.

- ➢ Composition and ratio of sulfides were key factors affecting catalytic activity.

- ➢ Combination of template synthesis and ion-exchange method was a feasible route to develop new composite photocatalysts.

1